Bisphenol A interferes with first shell formation and development of the serotoninergic system in early larval stages of Mytilus galloprovincialis

Angelica Miglioli, Teresa Balbi, Lydia Besnardeau, Remi Dumollard, Laura Canesi

*Graphical Abstract

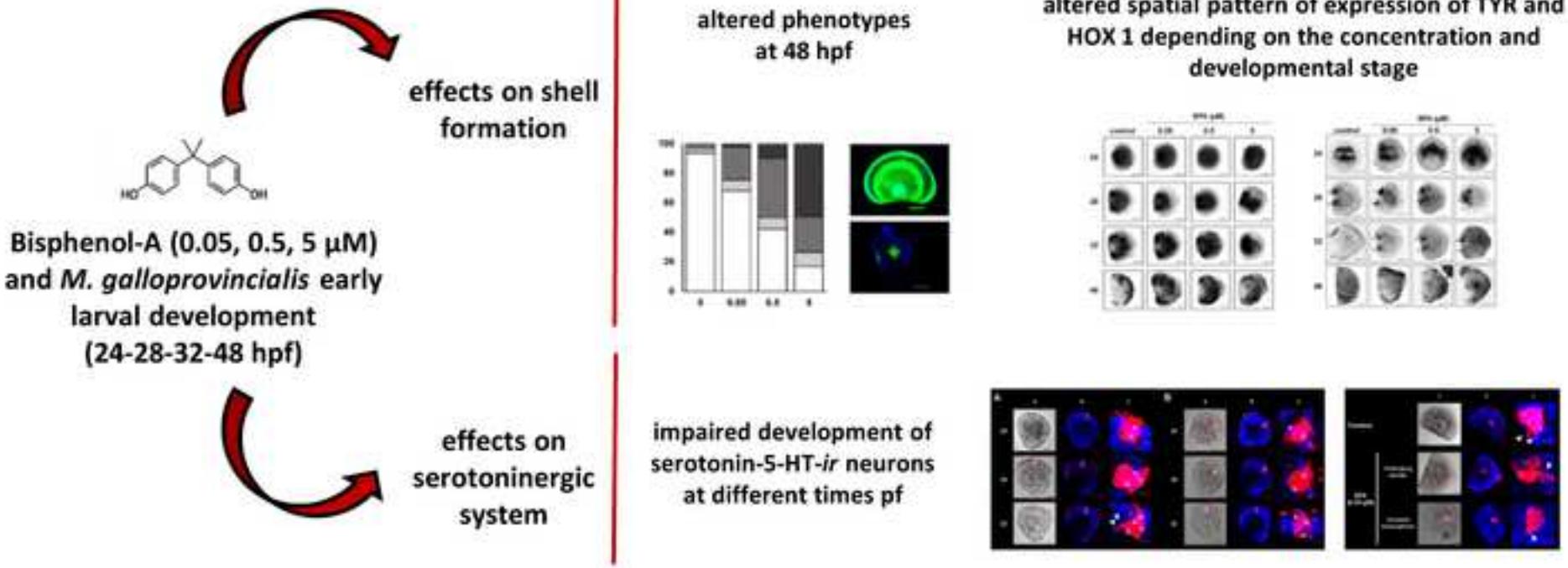

*Highlights (for review : 3 to 5 bullet points (maximum 85 characters including spaces per bullet point)

Highlights

- Bisphenol A-BPA affects early larval development in *Mytilus*
- Concentration dependent effects on deposition of organic matrix and $CaCO_3$
- Impact on transcription of genes involved in shell biogenesis Tyrosinase and HOX1
- Impaired development of serotonin(5-HT) neurons and changes in 5-HTR expression
- BPA interferes with shell formation and development of the serotoninergic system

Bisphenol A interferes with first shell formation and development of the serotoninergic system in early larval stages of *Mytilus galloprovincialis*

A. Miglioli[1,2], T. Balbi[1], L. Besnardeau[2] , R. Dumollard[2#], and L. Canesi[1#*]

[1]Dipartimento di Scienze della Terra, dell'Ambiente e della Vita, DISTAV, Università di Genova, Corso Europa 26, 16132 Genova, Italy

[2]Laboratoire de Biologie du Developpement de Villefranche-sur-mer, Institut de la mer, Sorbonne Université, CNRS, 181 Chemin du Lazaret, 06230 Villefranche-sur-mer, France

# These Authors equally contributed to the ms.

***Corresponding Author**

Laura Canesi

DISTAV, Università di Genova

Laura.Canesi@unige.it

Abstract

Bisphenol A-BPA, a widespread plastic additive, is an emerging contaminant of high concern and a potential endocrine disruptor in mammals. BPA also represents a potential threat for aquatic species, especially for larval stages. In the marine bivalve *Mytilus galloprovincialis*, BPA has been previously shown to affect early larval development and gene transcription. In this work, the effects of BPA (0.05-0.5-5 µM) were further investigated at different times post fertilization (24-28-32-48 hpf). BPA induced concentration-dependent alterations in deposition of the organic matrix and calcified shell at different larval stages, as shown by double calcofluor/calcein staining, resulting in altered phenotypes at 48hpf. Transcription of tTyrosinase-TYR, that plays a key role in remodelling of the shell organic matrix, and of HOX1, a member of homeobox genes involved in larval shell formation and neurogenesis, were evaluated by In Situ Hybrydization-ISH. BPA altered the spatial pattern of expression of both genes, with distinct effects depending on the concentration and developmental stage. Moreover, BPA affected the time course of mRNA levels for TYR from 24 to 48hpf. BPA impaired development of serotonin-5-HT-immunoreactive neurons at different times pf; at 48hpf, the reduction in the number of serotoninergic neurons was associated with developmental delay and downregulation of the 5-HT receptor-5-HTR. All the effects were observed from the lowest concentration tested, corresponding to detectable BPA levels in contaminated coastal waters. These data demonstrate that BPA interferes with key processes occurring during the first developmental stages of mussels, thus representing a potential threat for natural populations.

Keywords*: Bisphenol A, mussel, early development, shell formation, tyrosinase, hox1, serotonin*

1. Introduction

Bisphenol A (BPA), a monomer used in the production of epoxy resins and polycarbonate plastics is continuously produced and released into the environment in large quantities globally through sewage discharges, landfill leachate, surface runoff, and release from plastic debris. Although it degrades quickly, due to its continual inputs, it is pseudo-persistent and ubiquitous in different aquatic compartments, with reported concentrations between ng and µg/L (Flint et al., 2012; Canesi and Fabbri, 2015; Corrales et al., 2015; ECHA, 2017; Sousa et al., 2018; Staples et al., 2018; Wu and Seebacher, 2020). For freshwater, measurements are on average in the range between 10 and some 100 ng/l with mean maximum concentrations of 2000 ng/L for freshwater and above 8000 ng/L in marine waters (ECHA, 2017 and refs. therein). In Europe, concentrations of BPA were above detection limits in 70% and 61% of freshwater and marine water samples (Staples et al., 2018). BPA is weakly estrogenic and a potential endocrine disrupting chemical-EDC in mammals, and it also represents a potential concern for aquatic organisms, as shown by its reproductive and developmental effects on aquatic vertebrates and invertebrates, in particular on early life stages of molluscs and amphibians (Canesi and Fabbri, 2015; ECHA, 2017; Cuvillier-Hot and Lenoir, 2020; Wu and Seebacher, 2020). In July 2019, the General Court of the European Union confirmed that BPA must be listed as a substance of 'very high concern' (https://www.ehn.org/bisphenol-a-2639174350.html).

Marine invertebrates are sensitive to environmental stressors, especially during early larval stages. In addition, taxa characterized by calcified structures (e.g. molluscs, echinoderms) are markedly vulnerable to global changes, including ocean acidification and pollution (Hamdoun and Epel, 2007; Przeslawski et al., 2015). In this context, bivalve molluscs represent an important ecological group that, by living in complex environments such as coastal ecosystems, experience both natural environmental fluctuations (pH, temperature, salinity) and exposure to anthropogenic chemicals, and also show rapid adaptation capabilities to environmental fluctuations (Bitter et al., 2019). In the

mussel *Mytilus galloprovincialis*, BPA has been shown to affect early development in the 48h embryotoxicity assay in a wide concentration range (Fabbri et al., 2014). Further studies demonstrated that BPA, from nanoMolar concentrations, significantly affected transcription of several genes, including those involved in biomineralization and the serotonin receptor 5-HTR, both at the trocophora and D-veliger stage (24 and 48h pf post fertilization-pf, respectively) (Balbi et al., 2016). However, it is not known whether the observed changes in gene transcription induced by BPA are associated with impaired shell growth and formation of serotoninergic neurons, two key processes occurring during the first stages of larval development.

In *M. galloprovincialis*, the processes leading to the formation of the first larval shell have been recently investigated. The time course of both organic matrix and $CaCO_3$ deposition was evaluated, from the initial shell only made of organic matrix and characterized by a saddle shape (the shell field), to development of the first calcified larva, the D-veliger (Miglioli et al., 2019). These processes were associated with upregulation of genes involved in biomineralization (Tyrosinase, Chitin synthase, Carbonic anhydrase, Extrapallial Protein). In particular, the results underlined the pivotal role of tyrosinase in matrix deposition and remodelling and in driving first shell calcification (Miglioli et al., 2019).

In the present work, the effects of BPA (0.05, 0.5 and 5 µM) on the mechanisms involved in shell formation, and on the development of the serotoninergic system, were investigated in mussel larvae at close times pf (24, 28, 32, and 48h). Deposition of the organic matrix and of the calcified shell were evaluated by confocal imaging of Calcofluor/Calcein staining. The effect of BPA on larval phenotypes at 48hpf was also evaluated. Transcription of tyrosinase (TYR) was quantified by qPCR and its spatial pattern of expression by In Situ Hybridization-ISH. The effects of BPA on localization of transcripts for *M. galloprovincialis* Homeobox 1 (HOX1), a conserved transcription factor involved in ectodermal patterning and differentiation (Barucca et al., 2003; Perez-Parallè et al, 2005) and in molluscan larval shell formation and neurogenesis (Huan, et al. 2020) was also evaluated by ISH. Development of the serotoninergic system was investigated by evaluating

transcription of the serotonin receptors 5-HTR by qPCR and the presence of serotoninergic neurons by 5HT immunoreactivity.

2 Materials and Methods

2.1 Animal handling, gamete collection and fertilization

All procedures were carried out as previously described (Miglioli et al., 2019). and details are reported in SI. Fertilized eggs were exposed to different concentrations of BPA, depending on the endpoint measured (final concentrations 0.05, 0.5 and 5 µM, corresponding to 11.4, 114 and 1140 µg/L). These concentrations fall within the range previously utilized for evaluating the effects of BPA on mussel larval development at 48 hpf (Fabbri et al., 2014).

2.*2 Effect of Bisphenol A on formation of the first larval shell: morphometric analysis*

Fertilized eggs were exposed to BPA in 24-well plates at 30 min pf. Stock solutions of BPA (0.5 M in Dimethyl-sulfoxide/DMSO) were diluted in MFSW at 100 µM and tenfold serially diluted to obtain the desired concentrations (100 nM, 1 µM and 10 µM - 2x with respect to final concentration). The time-course of shell formation was investigated at different times pf, between the trochophore and the D-veliger stage (24, 28, 32 and 48 hpf). For details on early larval development see SI. Control samples in MFSW added with the vehicle at the final concentration utilized (0.01% DMSO) were run in parallel. Fluorescent dyes were employed to visualize the components of the larval shell as previously described (Miglioli et al., 2019): Calcofluor White Fluorescent Brightener 28 (Sigma Aldrich, Lyon, France) for organic matrix and Calcein (Sigma Aldrich, Lyon, France) for $CaCO_3$ deposition, respectively, as previously described (Miglioli et al., 2019) and details are reported in SI .

Larvae were imaged at each experimental time point with a Leica SP8 Confocal Laser Scanning Microscope (CLSM - Leica, France) scanning sequentially Calcofluor, Calcein and Brightfield signals with a 0.5 µm Z-stack interval. Channels were merged, 3D rendered and rotated to measure

the area (in μm^2) of one organic/calcified valve in each larva by manual drawing using IMAGEJ software (Kapsenberg et al., 2018). Area measurements were performed on larvae obtained from 5 independent parental pairs (N=5) and on least 15 individuals for each experimental condition. Data were normalized with respect to controls for each parental pair in different experimental conditions (times pf and exposure).

At 48 hpf, the effect of BPA was also evaluated by scoring shell malformations and measuring shell lengths in larvae from 5 independent parental pairs and in at least 50 larvae for each parental pair (see SI). *2.3 In situ hybridization – ISH*

The ISH protocol previously described for *M. galloprovincialis* larvae (Miglioli et al., 2019) was used to investigate the expression patterns of Mg-tyrosinase (Mg-Tyr, GenBank: KV583276.1) and Mg-Homeobox1A (Mg-HOX1A, GenBank: FN597580.1). Primer pairs were designed to amplify approximately 1-1.5 Kb cDNA fragment of Mg-Tyr (5'-ATGCGATTCTTTATACATGAAA-3';3'-TTGGTGGTTTTGGTACATGT-5') and Mg-HOX1A (5'-ATGAATACGGAGAGTGATTACACA-3'; 3'-TCGACTGTCCTGACATAAACCCAT-5'). The amplicons were then used to synthesize sense and antisense digoxigenin-labelled RNA probes as previously described (Miglioli et al., 2019). Larvae (control and BPA-exposed) were grown in 50 mL culture flasks as described above. At different times pf (24, 28, 32 and 48 h), larvae were sampled and concentrated with a 60 µm nylon filter, fixed overnight in 4% Paraformaldehyde in Phosphate Buffer Saline-PBS (137 mM NaCl, KCl 2.7 mM, 10 mM Na_2HPO_4, KH_2PO_4 1.8 mM, pH 7.4), washed in the same buffer and kept in 100% methanol at -20°C. Analyses were performed on larvae obtained from at least 4 independent parental pairs (100 individuals for each parental pair and experimental condition).

2.4 qPCR

Eggs were fertilized in polystyrene 6-well plates and treated with 2x BPA solution in order to obtain the final nominal concentration of 0.05 µM in a 8 mL volume. Control samples were run in parallel. Larvae were collected at 24, 28, 32 and 48 hpf by a nylon mesh (20 µm pore-filter) and washed

with artificial seawater (ASW) (Balbi et al., 2016). Three wells for each stage were pooled in order to obtain approximately 7000 embryos/replicate. RNA extraction, retro-transcription and qPCR were carried out as previously described (Balbi et al., 206; Miglioli et al., 2019) and are described in SI.

2.5 5-HT immunocytochemistry

Antibodies against the neurotransmitter serotonin (5-HT) were used to visualize the development of the serotonergic system in control, 0.05 and 0.5 µM BPA- exposed larvae at different times pf, using an adaptation of the protocols already available for larvae of other bivalves (Voronezhskaya et al., 2008, Yurchenko et al., 2018). Subsamples of larvae employed for ISH were used for 5-HT immunostaining. Larvae were rehydrated from 100% Methanol with 3 x 15 min washes in PBS, decalcified by treatment with 0.1 M Ethylenediaminetetraacetic acid (EDTA) in PBS for 1 h at room temperature-RT, and rinsed with 3 x 15 min washes in PBS. In order to eliminate non-specific binding sites, larvae were incubated overnight in Blocking Solution [10% normal goat serum, 0.25% bovine serum albumin (BSA), 0.03% sodium azide (NaN_3), PBS-Tx 1% (Triton X-100)] at 4° C. After 3 x 15 min washes in PBS-Tx 0.1%, larvae were soaked for 10 min at RT in the primary Antibody Buffer (1:10 Blocking Buffer in PBS), then added with a polyclonal primary antibody against Rabbit 5-HT (Immunostar, Hudson, WI, USA) at a final dilution 1:10.000 and incubated for 5 days at 4° C. After 3 x 1 h rinsing in PBS-Tx 0.1%, larvae were incubated for 3 days at 4°C with Goat Anti-Rabbit Rhodamine Red™-X (RRX) IgG secondary antibody (TRICT, Ex/Em: 570/590 nm - Jackson laboratory, Bar Harbor, Maine, USA) at a final dilution 1:500 in PBS-Tx 0.1%. Non-specific binding was evaluated in subsamples incubated only in the presence of the secondary antibody (not shown). Samples were rinsed with 3 x 1 h washes in PBS, stained with 1 µg/ml Hoechst in PBS (UV, Ex/Em: 352⁄461 nm- Hoechst 33342, Invitrogen) for 30 min at room temperature to visualize the nuclei, finally rinsed 3 x 15 min in PBS and mounted with glycerol phosphate buffered solution containing antifading agent (CitiFluor™ AF1, pH 10, Agar scientific). Embryos were imaged with a Leica Sp8 CLSM; Hoechst, 5-HT *(ir)* and Brightfield signals were

sequentially scanned with a 0.3 µm Z-stack interval. Using ImageJ software, channels were merged and subsequent Z-stacks were assembled in order to assess the number of immunoreactive (*ir*) cells by counting Hoechst stained nuclei in the 5-HT *ir* region as shown in Fig. S1.

2.6 Statistical analysis

All data, obtained from 5 or 4 independent parental pairs, depending on the experiment (mean ± SD) were analysed by one-way nonparametric ANOVA (Kruskal-Wallis test) followed by the Tukey's test ($p<0.05$). All statistical calculations were performed using GraphPad Prism 5 software (GraphPad Inc.).

3. Results

3.1 Effect of Bisphenol-A on shell biogenesis and larval development

Fertilized eggs were exposed to different concentrations of BPA (0.05, 0.5 and 5 µM) and the growth of the organic matrix and calcified shell was evaluated by morphometric analysis of stained larvae at different times pf, as previously described (Miglioli et al., 2019). In Fig. 1 representative images are reported of Calcofluor/Calcein staining in control larvae and larvae exposed to different concentrations of BPA (from left to right) at 24, 28, and 32hpf, showing the organic matrix (blue) and calcified component (green) of the growing shell. As previously described, in control samples at 24hpf, the initial larval shell was characterized by a saddle shape (the shell field) completely made of organic matrix, with no signs of calcification (Miglioli et al., 2019). BPA exposure induced alterations of the organic matrix, that was reduced to a thin line at the highest concentration tested (5 µM). At 28hpf, when first calcification was visible in control larvae, increasing concentrations of BPA induced changes in both structures. At 32hpf, control samples showed increased calcification, with evident accretion rings, while the hinge region was still not calcified. At this time point, all BPA concentrations affected the organic matrix as well as the calcified shell. In particular, larvae exposed to both 0.5 and 5 µM BPA had the typical appearance of immature stages, and no accretion rings were visible in the calcifying shell. At 48hpf, control larvae reached the normal D-veliger

193 stage, characterized by extensive calcification and a straight hinge. In BPA-exposed larvae, D-
194 veligers were also observed; however, lower concentrations of BPA induced shell malformations, in
195 particular in the hinge region, and also altered the pattern of calcification. At the highest
196 concentration tested (5 µM), BPA led to disruption of both shell matrix and $CaCO_3$ deposition.
197 The effects of BPA on the growth of organic matrix and calcified shell were quantified by
198 measuring the areas of each shell component (μm^2) as previously described (Miglioli et al., 2019).
199 Data are reported in Fig. 2, as % values recorded in BPA-exposed larvae with respect to controls at
200 24 (A), 28 (B) and 32hpf (C). At 24hpf, BPA induced a dose-dependent decrease of the area
201 occupied by the organic matrix (blue), that was significant at 0.5 and 5 µM BPA (-28% and 64%,
202 respectively; $p<0.05$ (Fig. 2A). A similar effect on the organic matrix was observed at 28 hpf (Fig.
203 2B). Moreover, at this stage BPA induced a concentration dependent decrease in the calcified areas
204 (green) that paralleled those observed for the organic matrix; such a decrease was significant at all
205 the concentrations tested (from -20% to -50% at 0.05 and 5 µM, respectively; $p<0.05$) (Fig. 2B).
206 Similar decreases in both shell components were observed at 32hpf at all the concentrations tested
207 (Fig. 2C), and they were associated with evident phenotypic changes (Fig. 1). The results are
208 summarized in Fig. 2D, where data are reported as organic matrix:calcified shell ratios in different
209 experimental conditions. In control larvae this ratio showed a significant decrease from 28 to 32
210 hpf, reflecting progressive calcification. BPA induced a concentration-dependent increase in the
211 area occupied by the organic matrix with respect to that of the calcified shell, indicating a delay in
212 $CaCO_3$ deposition.
213 In Fig. 3A main phenotypical alterations induced by BPA at 48 hpf are reported (malformed hinge,
214 protruding mantle, arrested trocophora). BPA induced a concentration dependent decrease in the
215 percentage of normal D-larvae (from 94% in controls to 18% at the highest BPA concentration)
216 (Fig. 3B). A small increase in the percentage of malformed shells (convex or indented hinge) was
217 observed with respect to the number of total larvae at all the concentrations tested (from a minimum
218 of 2.7% to a maximum of 9.4% in control and larvae exposed to 5 µM BPA. Moreover, a

progressive delay in development was observed, indicated by the increase in the proportion of immature D-veligers, characterized by protruding mantle, at all the concentrations tested (from 3.4% in controls to 25.7% in larvae exposed to 5 µM BPA). In addition, a clear concentration dependent increase in the proportion of larvae withheld at the trocophora stage was observed, reaching 50% of total larvae at the highest concentration tested. When the average shell length of all D-veligers (normal, malformed, immature) was measured, both 0.5 and 5 µM BPA also induced a significant decrease in size with respect to controls (Fig. 3C) ($p<0.05$).

3.2. Effect of BPA on gene expression in the shell field: tyrosinase and HOX1

After screening different genes involved in first shell formation (such as CS, CA, EP) (not shown), TYR and HOX1 were selected as possible targets for BPA on the basis of their localization in the area of the shell field (Miglioli et al., 2019; Pin Huan et al., 2020). Expression of tyrosinase (TYR) was first quantified by qPCR in control larvae and larvae exposed to the lowest concentration of BPA (0.05 µM). In Fig. 4, data on the time course of the level of TYR mRNA transcripts in control and BPA-exposed larvae at different times pf are reported with respect to eggs. In control larvae, a large upregulation was observed from 24hpf, that peaked at 32hpf (with an increase of about 8000-folds with respect to eggs), followed by a decrease at 48 hpf. Such trend was affected by exposure to BPA, that significantly increased TYR transcription at 24 and 32 hpf (+67% and +34 % compared to controls respectively, $p<0.05$). The effects of BPA on the TYR expression pattern were then evaluated by ISH (Fig. 5). As previously described (Miglioli et al., 2019) in larvae grown in physiological conditions, TYR was highly expressed in the shell field area from 24 hpf, and its localization subsequently paralleled the growth of the organic matrix as the trochophore developed into the first D-Veliger at 48 hpf, when the signal was weaker and restricted to the margins of the growing shell (Fig. 5, first column). At 24 and 28 hpf, lower concentrations of BPA (0.05 and 0.5 µM) did not significantly affect TYR expression pattern. However, from 32hpf, an altered spatial pattern was observed at all the concentrations tested, that was more evident at 48 hpf, when the

TYR signal was detected in the whole larval body. At the highest concentration (5 µM) BPA affected localization of TYR transcripts at all times pf.

ISH was also utilized to investigate the expression pattern of HOX1 mRNA and the results are reported in Fig. 6. In control larvae, HOX1 expression was highest at 24 hpf, when it was localized at the external margins of the shell field, but not in its centre, as clearly observed in the dorsal view of the larva. From 28 hpf, the signal was concentrated at two distinct, small areas along the hinge region (lateral view, black arrows), and it progressively weakened until becoming hardly detectable at 48hpf. BPA clearly affected HOX1 expression pattern at all times pf and at increasing concentrations. At 24 hpf, HOX1 transcripts progressively filled the centre of the shell field; at 28hpf the two distinct sites of expression (black arrows) were closer to each other until almost in contact in correspondence to the indented hinge at the highest concentration tested. At 32 hpf, BPA-exposed larvae showed a stronger signal (similar to that observed in control larvae at 28 hpf) indicating developmental delay, and the two sites of expression were closer with respect to controls. Finally, at 48 hpf, BPA apparently increased the HOX1 signal, but it strongly altered its pattern of expression in the whole larvae at all concentrations tested.

3.3 Effect of BPA on development of the serotonergic system

Levels of mRNA transcripts for the serotonin receptor 5-HTR were quantified by qPCR in control larvae and larvae exposed to BPA (0.05 µM) and data on the time course of 5-HTR transcription at different times pf are reported with respect to eggs in Fig. 7. In control samples, after a first upregulation at 24 hpf (about 150-folds with respect to eggs), a decrease in mRNA abundance for 5-HTR was observed at both 28 and 32 hpf, followed by strong upregulation at 48 hpf (about 700 folds vs eggs). BPA exposure did not affect transcription of 5-HTR between 24 and 32 hpf, whereas a significant decrease was observed at 48 hpf (-64% with respect to controls; $p<0.05$).

5-HT immunofluorescence labelling was utilized to detect serotonin positive cells by confocal microscopy, together with Hoechst staining to identify cell nuclei (Fig. S1), in control larvae and larvae exposed to 0.05 µM BPA at (24, 28, 32 and 48hpf). The results are reported in Fig. 8 and

271 Fig. 9, respectively. In control larvae 5-HT immunoreactivity (*ir*) was detectable from 24 hpf and it
272 was concentrated in few cells (Fig. 8A, columns a and b) that were located in the pre-trochal area of
273 the larva, close to the apical cilia (Fig. S2). As shown more detail in Fig 8A (column c), two 5-HT-
274 *ir* cells closely adjacent to each other could be identified in trochophora at 24hpf. As the larva
275 developed, the number of 5-HT-*ir* cells progressively increased to three at 28 hpf, and to four in the
276 late trocophora (32 hpf), where the emergence of tiny neurites could be also observed. In BPA-
277 exposed larvae 5-HT immunoreactivity, was clearly affected with respect to control larvae; in
278 particular, no more than two 5-HT-*ir* cells could be observed from the early to the late trocophora
279 stage (from 24 to 32 hpf) (Fig. 8B). At 48 hpf (Fig. 9), control D-veligers showed up to seven
280 serotonin positive neurons, organized into a compact pyramidal structure (columns a and b), and
281 emerging axons could be clearly identified expanding towards the hinge in the dorsal side of the
282 larva (Fig. 9A, column c). At this stage, in BPA-exposed larvae, different effects were observed
283 depending on the BPA-induced phenotype. In D-veligers showing protruding mantles, only five,
284 loosely connected 5-HT-*ir* cells were observed (column c). Moreover, ectopic 5-HT-*ir* cells were
285 occasionally observed in the protruding mantle (not shown). In arrested trocophorae, no more than
286 three 5-HT-*ir* neurons could be observed. Higher concentrations of BPA (0.5 µM) more severely
287 affected 5-HT immunoreactivity (Fig. S3 and Fig. S4). From 24 to 32 hpf, only one and two weakly
288 5-HT-*ir* cells could be observed (Fig. S3). At 48hf, a stronger reduction in 5-HT-*ir* cell number was
289 observed in malformed and immature D-veligers and in arrested trocophorae, where three, four and
290 two serotonin positive cells could be observed, respectively (Fig. S4).
291
292 **4. Discussion**
293 The results of this work obtained in the mussel *M. galloprovincialis* represent the first data on the
294 effects of BPA, a contaminant of emerging concern, on first shell formation and development of
295 serotoninergic system, two key processes of early larval development in bivalves. Different effects
296 of BPA could be observed from the lowest concentration tested (0.05 µM, corresponding to 11.4

297 µg/L), that falls within the environmental concentrations of BPA detected in some coastal areas
298 (Corrales et al., 2015).
299 Increasing concentrations of BPA affected the growth of both components of the shell (organic ma-
300 trix and $CaCO_3$ deposition), this mainly resulting in developmental delay. When the overall impact
301 of BPA on the growth of the two shell components was quantified by the organic matrix:calcified
302 shell ratio, a concentration and time dependent increase was observed at increasing times pf, indi-
303 cating an unbalance in the processes of shell formation. In particular, BPA induced alterations in the
304 pattern of deposition of both the organic matrix, that were progressively detectable from the early
305 trochophora stage, and of $CaCO_3$, with barely detectable shell accretion rings and non-
306 homogeneous calcification at later stages. These effects were reflected at 48 hpf by a concentration
307 dependent increase in the frequency and severity of altered shell phenotypes, resulting in develop-
308 mental arrest at the highest concentration tested. The double Calcofluor/Calcein staining, previous-
309 ly utilized to characterize the process of first shell formation in larvae grown in physiological condi-
310 tions (Miglioli et al., 2019) and in response to acidification (Kapsenberg et al., 2018), thus appears a
311 suitable method to evaluate not only phenotypical changes induced by chemical exposure, but also
312 to identify early contaminant-induced alterations in organic matrix deposition versus calcification.
313 With regards to the mechanisms involved in the effects of BPA, we have previously shown that,
314 among different genes involved in shell formation, tyrosinase was the most upregulated gene in
315 mussel early larval stages; moreover, TYR expression paralleled the formation of the shell field and
316 growth of the organic matrix from 24 hpf (Miglioli et al., 2019). These data indicated a key role of
317 this phenol oxidoreductase, in the early and progressive guiding of matrix deposition and shell
318 growth in *M. galloprovincialis*. The results obtained here show that in BPA exposed larvae the ef-
319 fects on shell growth were associated with quantitative and qualitative changes in transcription of
320 tyrosinase from 24 to 48hpf: from the lowest concentration tested, BPA affected both the time
321 course of transcription and the spatial pattern of expression of TYR, as shown by qPCR and ISH,
322 respectively. These data indicate expression of TYR, a key gene in matrix deposition, represents a

significant target for BPA in *Mytilus* early larval development. However, tyrosinases participate in the cross-linking and maturation of shell matrix proteins by catalysing the quinoprotein oxidation (Ren et al., 2020). Therefore, BPA may act on other process upstream of matrix deposition and more directly responsible for the initial shell patterning. Homeobox-containing genes play essential roles in the regulation of development and differentiation of many organisms. In particular, HOX genes, a subset of homeobox genes that encode transcription factors containing a highly conserved homeodomain-binding motif, are involved in anterior–posterior axial patterning and morphogenetic processes (Gehring et al., 1994). Several HOX genes have been identified in Mollusca; however, due to the vast diversity of body plans in each group (from bivalves to cephalopods), their functional role in development in each group is still to be elucidated (Huan et al., 2020). In gastropods, expression of HOX genes is initially detected in the trochophora shell field. Later, during development, these genes are expressed in the mantle, demonstrating their continuous role in larval shell formation and differentiation of mantle edge that secretes the adult shell (Samadi and Steiner, 2009, 2010). In bivalves, including *M. galloprovincialis*, different HOX genes have been identified (Barucca et al., 2003; Perez-Parallè et al, 2005); however, their role in development is still unknown. It has been recently proposed that HOX expression in the ventral ectoderm likely contributes to ventral patterning, such as neurogenesis, whereas HOX expression on the dorsal side is strongly correlated with shell formation and exhibits lineage-specific characteristics in each class of mollusc (Huan et al., 2020). Here we show that in *M. galloprovincialis* HOX1 was strongly expressed at 24 hpf in the dorsal side of the trocophora around the shell field, but not in its centre, and expression progressively declined at longer times pf. Exposure to BPA, from environmental concentrations clearly induced dose-dependent alterations in the transcription pattern of HOX1 at all times pf. Although other *Mytilus* HOX genes will participate in larval development, these results clearly show that expression of HOX1, a transcription factor involved in ectodermal patterning, is concentrated in the shell field, thus supporting its role in initial shell formation, and that it represents a significant

target for BPA during larval development. These results support the hypothesis that BPA can affect shell biogenesis from the very beginning of the morphogenetic process.

Previous data showed that both BPA and the natural estrogen 17β-estradiol (at 10 µg/L, a concentration close to the lowest utilized in the present work) could also affect neuroendocrine signalling in early larvae, including transcription of the serotonin receptor 5-HTR (Balbi et al., 2016). When transcription of 5-HTR was evaluated in control larvae, upregulation was observed at all times pf with respect to eggs, with highest levels of mRNA transcripts in early trocophorae and D-veligers (at 24 and 48 hpf, respectively). BPA induced significant downregulation of 5-HTR only at 48 hpf, confirming previous data (Balbi et al., 2016). In order to evaluate if BPA could affect development of the serotoninergic system, we looked for the presence of 5-HT immunoreactive neurons. In bivalves, neurogenesis begins with the emergence of the apical sensory cells (Voroneskaya et al., 2008 and refs. quoted therein). In *M. trossulus*, the earliest 5-HT immunoreactive (5-HT-*ir*) neuron was detected in the trochophora in the region of the developing apical organ (AO), the most conserved larval sensory structure, which later becomes a part of the emerging cerebral ganglion (Voronezhskaya et al., 2008). In different bivalve species, the AO develops from early trochophora where it consists of both 5-HT*ir* and FMRFamide *ir* cells (Voronezhskaya et al., 2008; Yurchenko et al., 2018; Pavlicek et al., 2018). In *M. trossulus* and *Crassostrea gigas*, the AO consists of three and five 5-HT*ir* cells in trochophorae and in D-veligers, respectively (Voronezhskaya et al., 2008; Yurchenko et al., 2018). Our data show that in control larvae of *M. galloprovincialis*, from the appearance of two 5-HT-*ir* cells in early trocophora at 24 hpf, the number of serotonin positive neurons progressively increased up to seven at 48 hpf, with the appearance of tiny neurites. These are the first results on the identification of 5-HT*ir* neurons in the AO of *M. galloprovincialis* early larval stages. The higher number of 5-HT-*ir* neurons detected in the present work with respect to previous studies in other bivalves is probably due to the utilization of the nuclear staining and 3D confocal imaging, which allows a more accurate cell counting on sequential z-stacks of 5-HT-*ir* and Hoechst merged fluorescence signals (Fig. S1).

374 Exposure to, environmental concentrations of BPA affected the development of 5-HT-*ir* neurons.
375 A decrease in the number of 5-HT-*ir* cells was detected from 28hpf. At 48 hpf, the extent of
376 reduction in cell number was associated with different degrees of developmental delay (from seven
377 in normal D-veligers, to five in early veligers and three in larvae withheld at the trocophora stage,
378 respectively). Higher concentrations resulted in even stronger reductions in the number of serotonin
379 positive neurons, that also in this case were associated with altered phenotypes at 48hpf
380 (malformed, immature, arrested).
381 The results demonstrate that in mussels exposure to BPA interferes with the development of another
382 ectodermal structure, i.e. neurogenesis of the serotoninergic system. Although the reduction in
383 number 5-HT-*ir* cells was detectable from the trocophora stages, the most evident effects were
384 detected at 48 hpf, when both the number of 5-HT-*ir* cells and the amount of 5-HTR transcripts
385 were reduced. Overall, the results indicate that exposure to BPA can induce neurodevelopmental
386 toxicity in *M. galloprovincialis*.
387 Current knowledge about the correlation between developmental exposure to BPA and levels of 5-
388 HT is relatively scarce. In mammalian models, it has been proposed that early life exposure to BPA
389 may alter the metabolism of 5-HT and other neurotransmitters, causing neurodevelopmental
390 disorders and behavioural defects (Castro et al., 2015; Xin et al., 2018). In male zebrafish, BPA-
391 induced behavioural changes were associated with reduced levels of 5-HT in the hypothalamus and
392 down-regulation of tyrosine hydroxylase in brain tissues (Li et al., 2017). In molluscs, 5-HT
393 signalling is involved in a number of key physiological processes from reproduction, to
394 neurogenesis and muscle contraction (Joyce and Vogeler 2018; Kim et al., 2019; Yurchenko et al.,
395 2019; Sharker et al., 2019); consequently, exposure to BPA during early life stages may interfere
396 with the onset of the serotoninergic system with potentially dramatic outcomes in wildlife
397 populations. Moreover, BPA may affect other components involved in development of the
398 neuroendocrine systems, such as FMRFamide or other neurotransmitters.

Overall the results indicate that in *Mytilus* early larval stages exposure to BPA can have a significant impact not only on initial shell formation but also on development of the nervous system, indicating that this compound can act through pleiotropic mechanisms. Further research is needed to investigate the mechanisms of action of BPA on different target cells of developing larvae and the possible relationship between the two processes. A recent study showed that, in early oyster larvae, shell formation was modulated by monoamine neurotransmitters 5-HT and dopamine (DA) through TGF-β smad pathway, triggering the expression of tyrosinase to form initial shell (Liu et al., 2020). In this light, it is tempting to hypothesize that exposure to BPA may directly affect the metabolism of 5-HT (or other monoamines like DA), leading to dysregulation of organic matrix deposition and consequent calcification. Thus BPA has a strong neurodevelopmental impact in bivalves. However, it remains to be shown whether the effects of BPA exposure could be reversed after subsequent recovery to clean conditions or by other environmental factors. Increasing knowledge on the first steps of physiological larval development in different bivalve species may help identifying early signs of impact of different environmental stressors, from exposure to emerging contaminants to ocean acidification, thus contributing to a better understanding of potential perturbation of developmental processes of marine invertebrates in a global change scenario.

Acknowledgments

The authors would like to thank Laurent Gilletta, Alexandre Jean,Régis Lasbleiz and the Centre de Ressources Biologiques Marines of the CRBM-IMEV that is supported by EMBRC-France, whose French state funds are managed by the Agence Nationale de la Recherche (ANR) withi the 'Investissement d'Avenir' program (ANR-10-INBS-02); Sameh Benaicha; the Ascidian BioCell group members. The experiments performed in the laboratory of R.D. were financed by an ANR grant (Marine-EmbryoTox project, ANR-14-OHRI-0009-01-1).

Figure Legends

Figure 1 - Effect of Bisphenol-A (0.05, 0.5 and 5 µM) on the time course of early shell formation in *M. galloprovincialis* from the trochophora to the first D-veliger stage at different times post-fertilization (from top to bottom: at 24, 28, 32, 48 hpf). Columns correspond to experimental conditions (from left to right: Control, 0.05, 0.5, 5 µM BPA). Representative images (lateral view) show merged fluorescent signals of calcofluor (blue) and calcein (green) staining, respectively, the organic matrix and $CaCO_3$ deposition. (Scale bars: 10 µm).

Figure 2 - Effect of BPA (0.05, 0.5 and 5 µM) on the growth of organic matrix (blue) and calcified shell (green) in mussel larvae. Areas of each shell component (μm^2) measured in a single valva of BPA-exposed larvae are reported as % values of control (unexposed) larvae at 24 (A), 28 (B) and 32 hpf (C). In D) ratios of areas matrix/calcified shell in different experimental conditions are reported. Measurements were made on 15 larvae for each condition obtained from 5 parental pairs (N=5). * $p \leq 0.05$, BPA-exposed *vs* Controls; # Control 28 hpf *vs* 32 hpf (one way ANOVA Kruskall-Wallis followed by Tukey's test).

Figure 3 - Effect of BPA (0.05, 0.5 and 5 µM) on shell morphology at 48 hpf.
A) representative images of control larvae and of the main phenotypes observed in BPA-exposed larvae (scale bar: 20 µm). B) percentage of different phenotypes: normally developed D-Veligers (white), with hinge malformations (light gray), with extruding mantle (dark grey) and arrested to the trochophora stage (black). C) Shell length of D-veligers, i.e. the anterior-posterior dimension of the shell parallel to the hinge line normalized as % of controls (Inset), * $p \leq 0.05$. Measurements were made on 70 larvae for each experimental condition obtained from 5 parental pairs (N=5).

Figure 4 - Time course of tyrosinase (TYR) expression in control and BPA-exposed larvae of *M. galloprovincialis* evaluated by qPCR at different times pf. Data, reported as fold changes with respect to eggs, represent the mean ± SD (N=4). Data were analysed by one way ANOVA Kruskall-Wallis followed by Tukey's test and statistical differences between control and BPA-exposed samples at each developmental stage are reported (* $p < 0.01$). Expression of all transcripts was significantly different at all times pf with respect to eggs ($p < 0.01$, not shown).

Figure 5 - Effect of Bisphenol A on TYR expression pattern evaluated by ISH in mussel larvae from 24 to 48 hpf.

Columns (from left to right: Control, 0.05, 0.5 and 5 µM BPA); rows (from top to bottom: 24, 28, 32, 48 hpf). Scale bar: 20 µm

Figure 6 - HOX1 expression pattern evaluated by ISH in mussel larvae.

A) Control larvae at 24, 28, 32, 48 hpf (lateral view); B) Effect of BPA 0.05, 0.5 and 5 µM at 24 hpf (dorsal view). The red line indicates the perimeter of the shell field. Scale bar: 20 µm.

Figure 7 - Transcriptional profile of the serotonin receptor (5-HTR) during early larval development in *M. galloprovincialis* evaluated by qPCR at different times pf. Data, reported as fold changes with respect to eggs, represent the mean ± SD (N=4). Data were analysed by 1-way non-parametric ANOVA plus Tukey's test and statistical differences between control and BPA-exposed samples at each developmental stage are reported (* $p<0.01$). Expression of all transcripts was significantly different at all times pf with respect to eggs (one way ANOVA followed by Tukey's test; $p < 0.01$, not shown).

Figure 8 - Confocal images of serotonin immunoreactive cells (5-HT-*ir*) in early larval stages of *M. galloprovincialis* from 24 to 32 hpf. A) control; B) BPA-exposed (0.05 µM).

5-HT-*ir* cells are shown in Red/Pink (Ex/Em: 590/617 nm), DAPI stained nuclei are shown in blue (Ex/Em: 358⁄461 nm). Rows correspond to hours post fertilization: 24, 28, 32 hpf. Columns show:

a) brightfield and 5-HT merged channels, scale bar: 20 µm;

b) 5-HT and DAPI merged channels, scale bar: 20 µm.

c) 4-5 X magnified images of column B: white asterisks indicate the nuclei of 5-HT-*ir* cells (*) and white arrowheads emerging neurites, respectively, scale bar: 5 µm.

A) In control larvae, 5-HT immunoreactivity was concentrated in compact developing neurons from 24 hpf. In column c) the presence of two, three, and four-five 5-HT-*ir* cells can be identified, respectively, from 24 to 32 hpf (*).

B) In larvae exposed to BPA (0.05 µM), 5-HT immunoreactivity was apparently more scattered. Moreover, only two 5-HT-*ir* cells could be observed from 24 to 32 hpf.

Figure 9

Confocal images of serotonin immunoreactive cells (5-HT-*ir*) in control and BPA-exposed early larval stages of *M. galloprovincialis* at 48 hpf**.** All details as in Fig. 8.

In A) and B) images of control and BPA-exposed larvae are reported, showing representative BPA-induced phenotypes and 5-HT immunoreactivity, respectively, scale bars: 20 µm.

In C) details are reported showing that BPA-induced phenotypic alterations are associated with a reduction in the number of 5-HT-*ir* cells (*); arrowheads indicate emerging neurites. Scale bar: 5 µm.

498 References

499 1. ASTM Standard E724-98, 2012. Guide for Conducting Static Acute Toxicity Tests Starting
500 with Embryos of Four Species of Saltwater Bivalve Molluscs. ASTM International, West
501 Conshohocken, PA.

502 2. Balbi, T., Franzellitti, S., Fabbri, R., Montagna, M., Fabbri, E., Canesi, L., 2016. Impact of
503 bisphenol A (BPA) on early embryo development in the marine mussel Mytilus
504 galloprovincialis: Effects on gene transcription. Environmental Pollution 218, 996–1004.
505 https://doi.org/10.1016/j.envpol.2016.08.050

506 3. Barucca, M., Olmo, E., Canapa, A., 2003. Hox and paraHox genes in bivalve molluscs.
507 Gene 317, 97–102. https://doi.org/10.1016/s0378-1119(03)00657

508 4. Bitter, M.C., Kapsenberg, L., Gattuso, J.-P., Pfister, C.A., 2019. Standing genetic variation
509 fuels rapid adaptation to ocean acidification. Nature Communications 10.
510 https://doi.org/10.1038/s41467-019-13767-1

511 5. Canesi, L., Fabbri, E., 2015. Environmental Effects of BPA. Dose-Response 13,
512 155932581559830. https://doi.org/10.1177/1559325815598304

513 6. Castro, B., Sánchez, P., Miranda, M. T., Torres, J. M., & Ortega, E. (2015). Identification of
514 dopamine- and serotonin-related genes modulated by bisphenol A in the prefrontal cortex of
515 male rats. Chemosphere, 139, 235–239. https://doi.org/10.1016/j.chemosphere.2015.06.061

516 7. Corrales, J., Kristofco, L.A., Steele, W.B., Yates, B.S., Breed, C.S., Williams, E.S., Brooks,
517 B.W., 2015. Global Assessment of Bisphenol A in the Environment. Dose-Response 13,
518 155932581559830. https://doi.org/10.1177/1559325815598308

519 8. Cuvillier-Hot, V., Lenoir, A., 2020. Invertebrates facing environmental contamination by
520 endocrine disruptors: Novel evidences and recent insights. Molecular and Cellular
521 Endocrinology 504, 110712. https://doi.org/10.1016/j.mce.2020.110712

522 9. ECHA (2017). Agreement Of The Member State Committee On The Identification Of 4,4'-
523 Isopropylidenediphenol (Bisphenol A) As A Substance Of Very High Concern According
524 To Articles 57 And 59 Of Regulation (Ec) 1907/20061. Adopted on 14 June 2017.
525 Available at

https://www.echa.europa.eu/documents/10162/13638/svhc_msc_agreement_bpa_ii_en.pdf/ac9efb97-c06b-d1a7-2823-5dc69208a238.

10. Fabbri, R., Montagna, M., Balbi, T., Raffo, E., Palumbo, F., Canesi, L., 2014. Adaptation of the bivalve embryotoxicity assay for the high throughput screening of emerging contaminants in Mytilus galloprovincialis. Marine Environmental Research 99, 1–8. https://doi.org/10.1016/j.marenvres.2014.05.007

11. Flint, S., Markle, T., Thompson, S., Wallace, E., 2012. Bisphenol A exposure, effects, and policy: A wildlife perspective. Journal of Environmental Management 104, 19–34. https://doi.org/10.1016/j.jenvman.2012.03.021

12. Gehring, W.J., Qian, Y.Q., Billeter, M., Furukubo-Tokunaga, K., Schier, A.F., Resendez-Perez, D., Affolter, M., Otting, G., Wüthrich, K., 1994. Homeodomain-DNA recognition. Cell 78, 211–223. https://doi.org/10.1016/0092-8674(94)90292-5

13. Hamdoun, A., Epel, D., 2007. Embryo stability and vulnerability in an always changing world. Proceedings of the National Academy of Sciences 104, 1745–1750. https://doi.org/10.1073/pnas.0610108104

14. Huan, P., Liu, G., Wang, H., Liu, B., 2013. Identification of a tyrosinase gene potentially involved in early larval shell biogenesis of the Pacific oyster Crassostrea gigas. Development Genes and Evolution 223, 389–394. https://doi.org/10.1007/s00427-013-0450-z

15. Huan, P., Wang, Q., Tan, S., Liu, B., 2019. Dorsoventral decoupling of Hox gene expression underpins the diversification of molluscs. Proceedings of the National Academy of Sciences 117, 503–512. https://doi.org/10.1073/pnas.1907328117

16. Joyce, A., Vogeler, S., 2018. Molluscan bivalve settlement and metamorphosis: Neuroendocrine inducers and morphogenetic responses. Aquaculture 487, 64–82. https://doi.org/10.1016/j.aquaculture.2018.01.002

17. Kim, K.S., Kim, M.A., Sohn, Y.C., 2019. Molecular characterization, expression analysis, and functional properties of multiple 5-hydroxytryptamine receptors in Pacific abalone (Haliotis discus hannai). General and Comparative Endocrinology 276, 52–59. https://doi.org/10.1016/j.ygcen.2019.03.001

18. Li, X., Sun, M.-Z., Li, X., Zhang, S.-H., Dai, L.-T., Liu, X.-Y., Zhao, X., Chen, D.-Y., & Feng, X.-Z. (2017). Impact of low-dose chronic exposure to Bisphenol A (BPA) on adult male zebrafish adaption to the environmental complexity: Disturbing the color preference patterns and reliving the anxiety behavior. Chemosphere, 186, 295–304. https://doi.org/10.1016/j.chemosphere.2017.07.164

19. Liu, Z., Zhou, Z., Zhang, Y., Wang, L., Song, X., Wang, W., Zheng, Y., Zong, Y., Lv, Z., & Song, L. (2020). Ocean acidification inhibits initial shell formation of oyster larvae by suppressing the biosynthesis of serotonin and dopamine. Science of The Total Environment, 735, 139469. https://doi.org/10.1016/j.scitotenv.2020.139469

20. Miglioli, A., Dumollard, R., Balbi, T., Besnardeau, L., Canesi, L., 2019. Characterization of the main steps in first shell formation in Mytilus galloprovincialis : possible role of tyrosinase. Proceedings of the Royal Society B: Biological Sciences 286, 20192043. https://doi.org/10.1098/rspb.2019.2043

21. Page, L. R., & Kempf, S. C. (2009). Larval apical sensory organ in a neritimorph gastropod, an ancient gastropod lineage with feeding larvae. Zoomorphology, 128(4), 327–338. https://doi.org/10.1007/s00435-009-0093-9

22. Pavlicek, A., Schwaha, T., & Wanninger, A. (2018). Towards a ground pattern reconstruction of bivalve nervous systems: neurogenesis in the zebra mussel Dreissena polymorpha. Organisms Diversity & Evolution, 18(1), 101–114. https://doi.org/10.1007/s13127-017-0356-0

23. Pérez-Parallé, M.L., Carpintero, P., Pazos, A.J., Abad, M., Sánchez, J.L., 2005. The HOX Gene Cluster in the Bivalve Mollusc Mytilus galloprovincialis. Biochemical Genetics 43, 417–424. https://doi.org/10.1007/s10528-005-6780-4

24. Przeslawski, R., Byrne, M., Mellin, C., 2015. A review and meta-analysis of the effects of multiple abiotic stressors on marine embryos and larvae. Global Change Biology 21, 2122–2140. https://doi.org/10.1111/gcb.12833

25. Ren, G., Chen, C., Jin, Y., Zhang, G., Hu, Y., Shen, W., 2020. A Novel Tyrosinase Gene Plays a Potential Role in Modification the Shell Organic Matrix of the Triangle Mussel Hyriopsis cumingii. Frontiers in Physiology 11. https://doi.org/10.3389/fphys.2020.00100

584 26. Samadi, L., Steiner, G., 2009. Involvement of Hox genes in shell morphogenesis in the
585 encapsulated development of a top shell gastropod (Gibbula varia L.). Development Genes
586 and Evolution 219, 523–530. https://doi.org/10.1007/s00427-009-0308-6

587 27. Samadi, L., Steiner, G., 2010. Expression of Hox genes during the larval development of the
588 snail, Gibbula varia (L.)—further evidence of non-colinearity in molluscs. Development
589 Genes and Evolution 220, 161–172. https://doi.org/10.1007/s00427-010-0338-0

590 28. Schmittgen, T.D., Livak, K.J., 2008. Analyzing real-time PCR data by the comparative CT
591 method. Nature Protocols 3, 1101–1108. https://doi.org/10.1038/nprot.2008.73

592 29. Sharker, M.R., Sukhan, Z.P., Kim, S.C., Lee, W.K., Kho, K.H., 2019. Identification,
593 characterization, and expression analysis of a serotonin receptor involved in the reproductive
594 process of the Pacific abalone, Haliotis discus hannai. Molecular Biology Reports 47, 555–
595 567. https://doi.org/10.1007/s11033-019-05162-2

596 30. Sousa, A.C., 2018. Environmental contaminants and endocrine disruption: the story of
597 obesogens. Endocrine Abstracts. https://doi.org/10.1530/endoabs.56.s4.3

598 31. Staples, C., van der Hoeven, N., Clark, K., Mihaich, E., Woelz, J., Hentges, S., 2018.
599 Distributions of concentrations of bisphenol A in North American and European surface
600 waters and sediments determined from 19 years of monitoring data. Chemosphere 201, 448–
601 458. https://doi.org/10.1016/j.chemosphere.2018.02.175

602 32. Voronezhskaya, E.E., Nezlin, L.P., Odintsova, N.A., Plummer, J.T., Croll, R.P., 2008.
603 Neuronal development in larval mussel Mytilus trossulus (Mollusca: Bivalvia).
604 Zoomorphology 127, 97–110. https://doi.org/10.1007/s00435-007-0055-z

605 33. Wu, N.C., Seebacher, F., 2020. Effect of the plastic pollutant bisphenol A on the biology of
606 aquatic organisms: A meta- analysis. Global Change Biology.
607 https://doi.org/10.1111/gcb.15127

608 34. Xin, F., Fischer, E., Krapp, C., Krizman, E. N., Lan, Y., Mesaros, C., … Bartolomei, M. S.
609 (2018). Mice exposed to bisphenol A exhibit depressive-like behavior with neurotransmitter
610 and neuroactive steroid dysfunction. Hormones and Behavior, 102, 93–104.
611 https://doi.org/10.1016/j.yhbeh.2018.05.010

35. Yang, B., Pu, F., Li, L., You, W., Ke, C., Feng, D., 2017. Functional analysis of a tyrosinase gene involved in early larval shell biogenesis in Crassostrea angulata and its response to ocean acidification. Comparative Biochemistry and Physiology Part B: Biochemistry and Molecular Biology 206, 8–15. https://doi.org/10.1016/j.cbpb.2017.01.006

36. Yurchenko, O. V., Skiteva, O. I., Voronezhskaya, E. E., & Dyachuk, V. A. (2018). Nervous system development in the Pacific oyster, Crassostrea gigas (Mollusca: Bivalvia). Frontiers in Zoology, 15(1). https://doi.org/10.1186/s12983-018-0259-8

37. Yurchenko, O.V., Savelieva, A.V., Kolotuchina, N.K., Voronezhskaya, E.E., Dyachuk, V.A., 2019. Peripheral sensory neurons govern development of the nervous system in bivalve larvae. EvoDevo 10. https://doi.org/10.1186/s13227-019-0133-6

Figure1

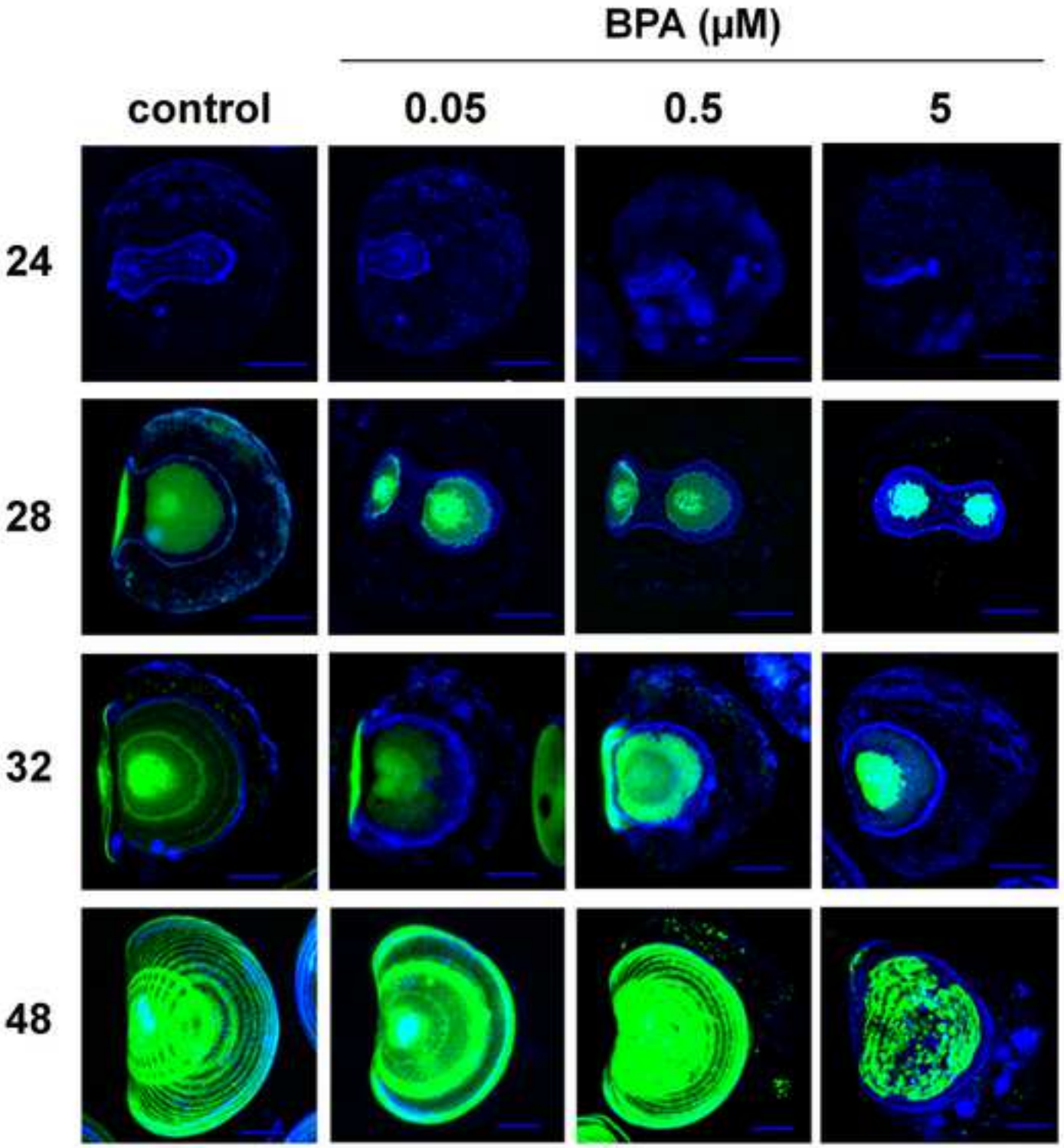

Figure2

Click here to access/download;Figure;Fig. 2.tif

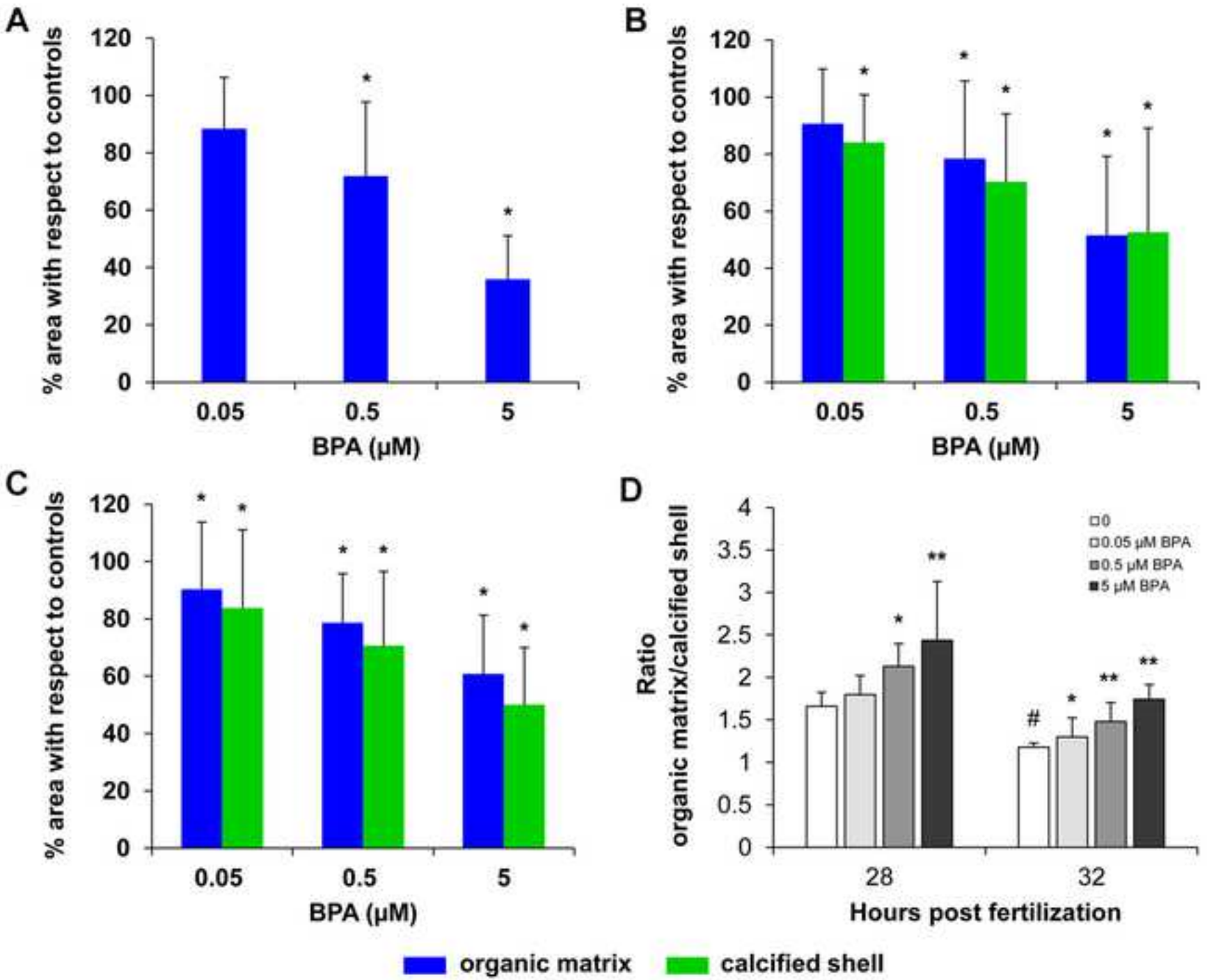

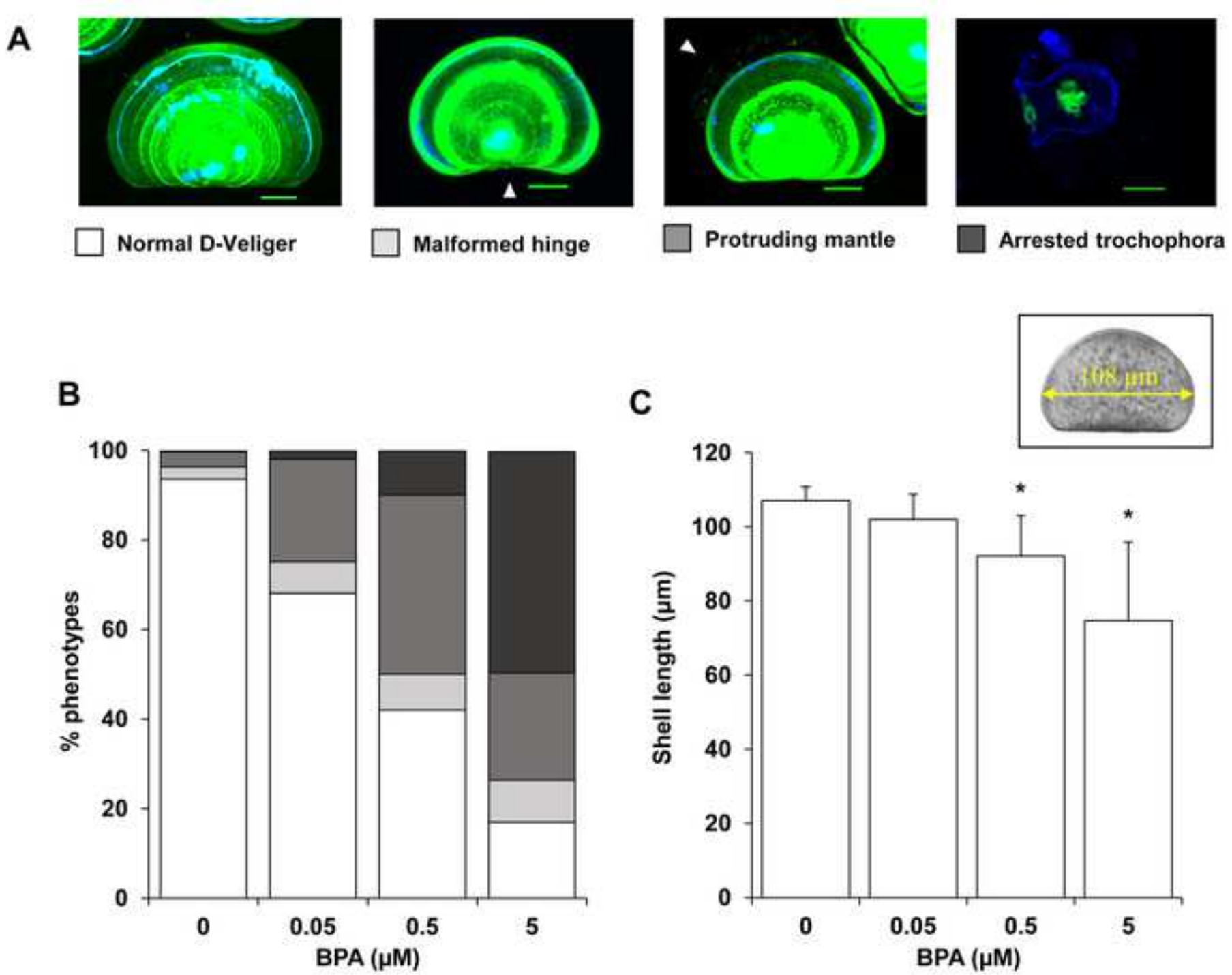

Figure4

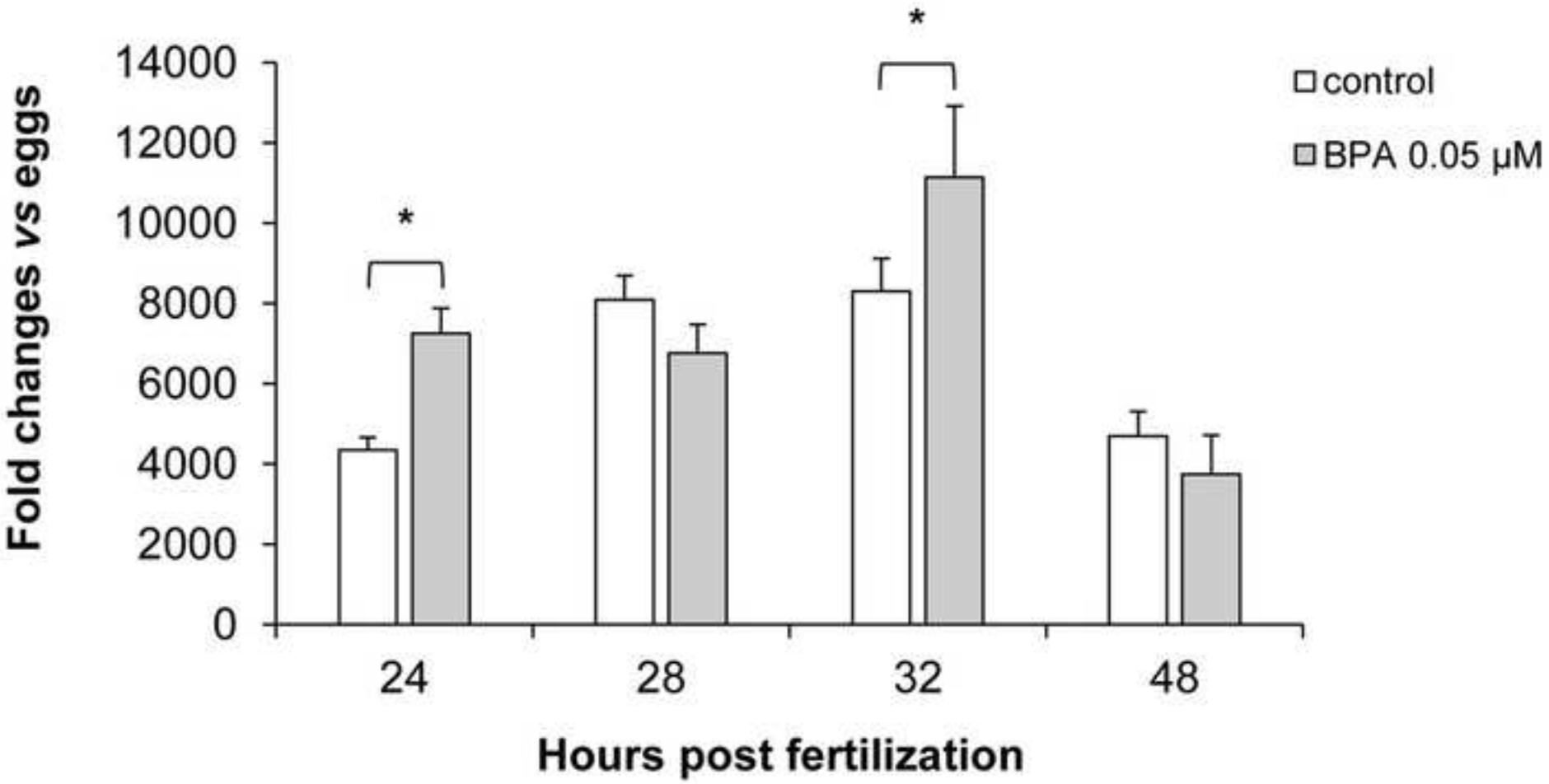

Figure5

Click here to access/download;Figure;Fig. 5.tif

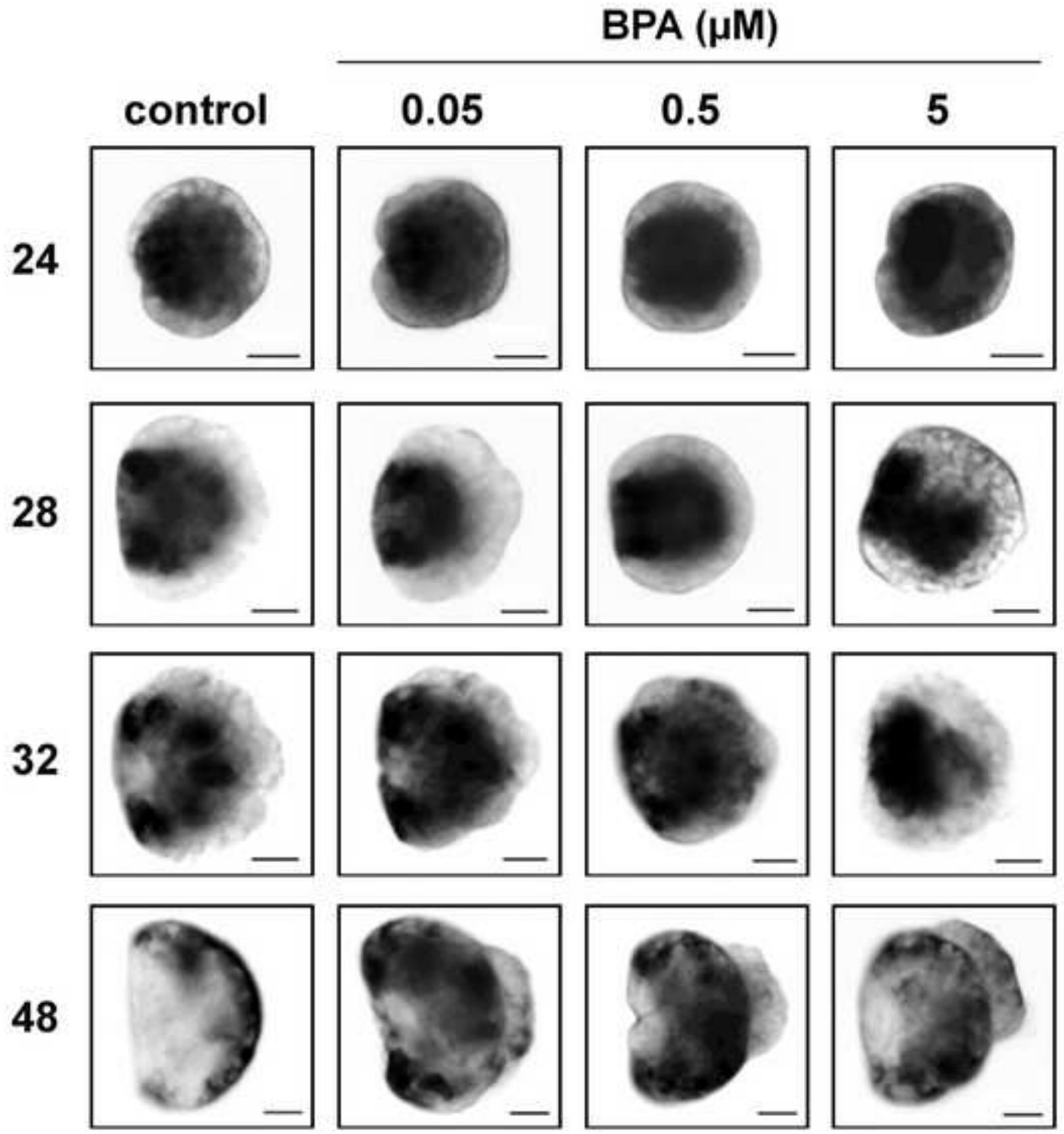

Figure6

Click here to access/download;Figure;Fig. 6.tif

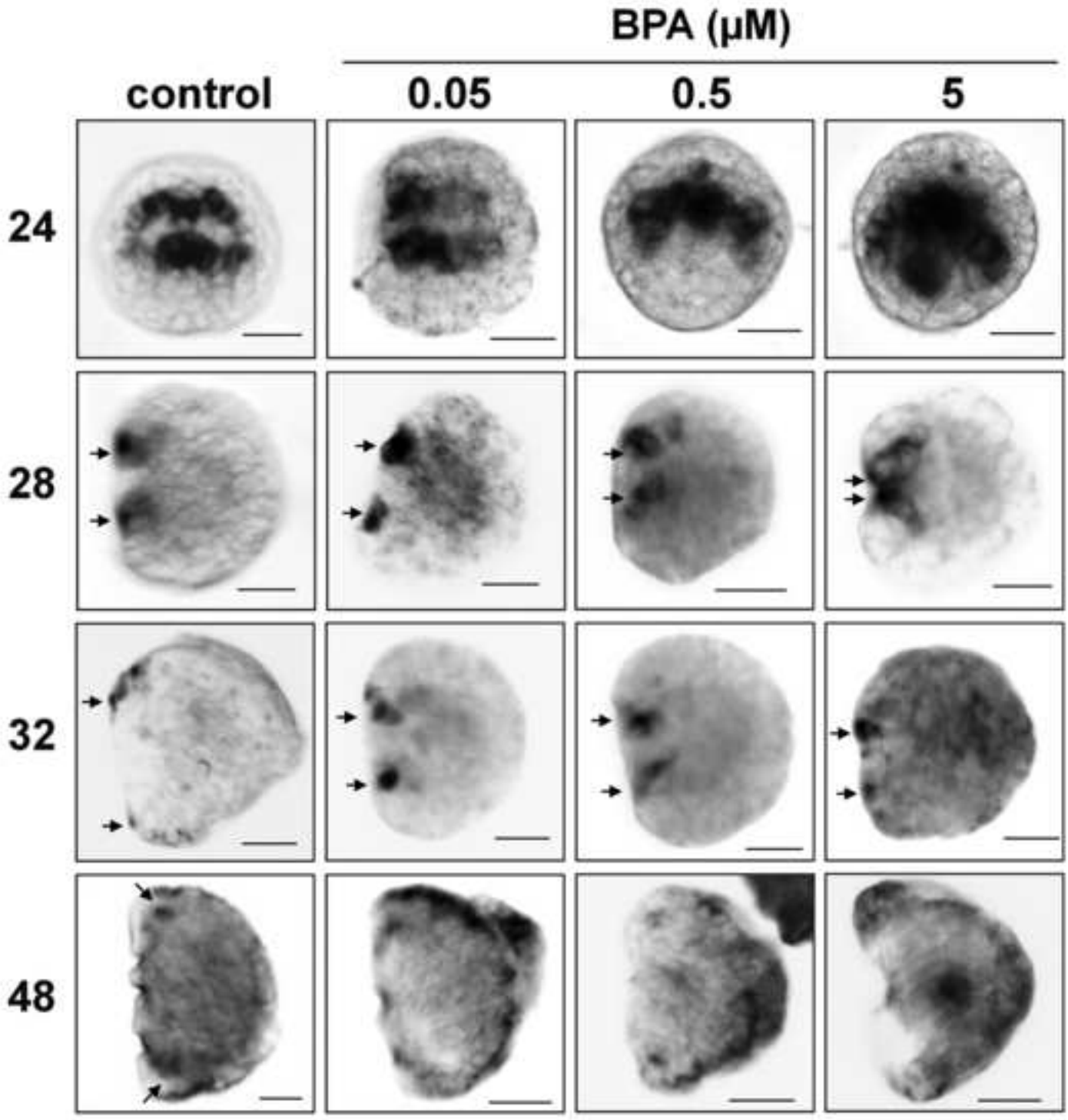

Figure7

Click here to access/download;Figure;Fig. 7.tif

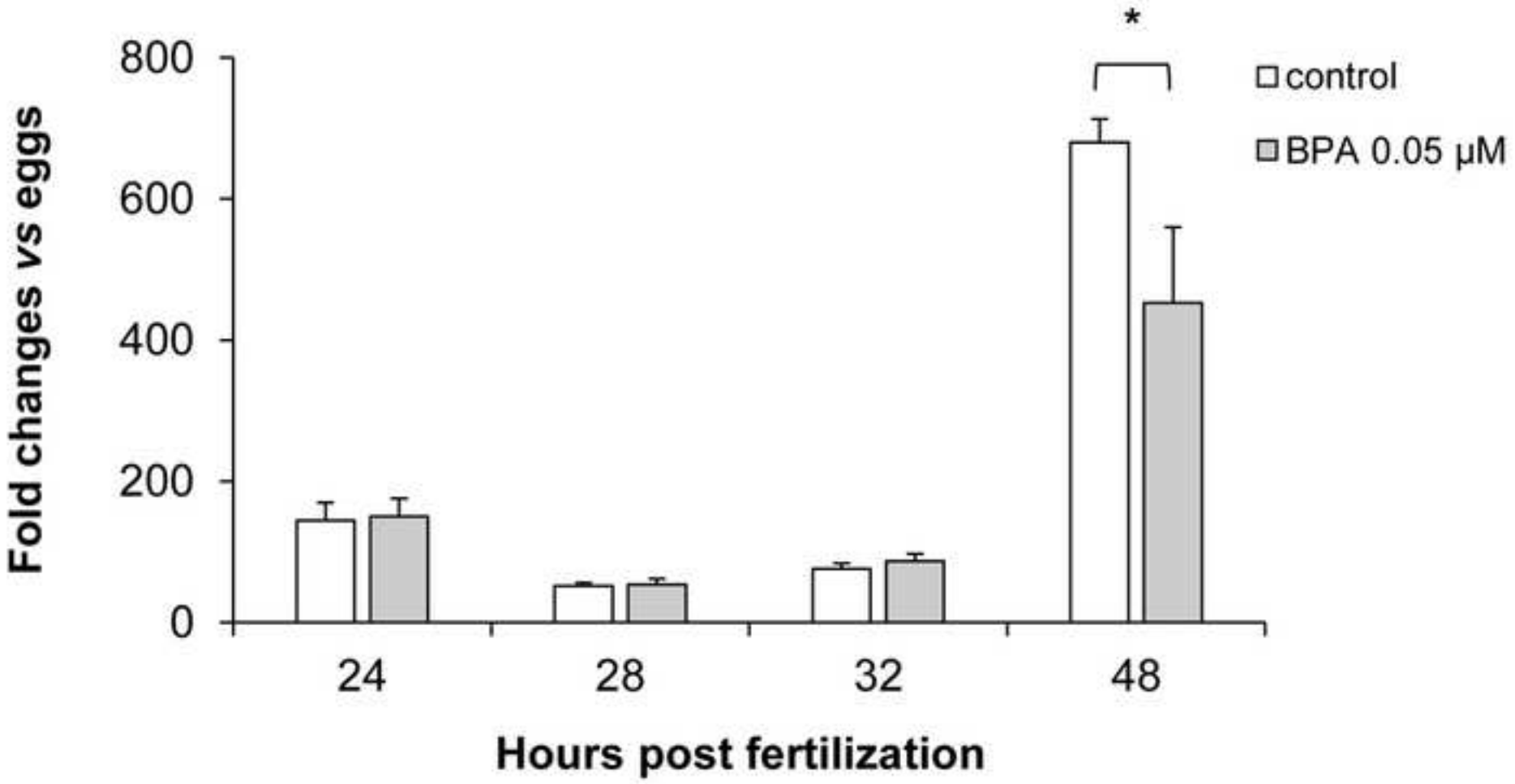

Figure8

Click here to access/download;Figure;Fig. 8.tif

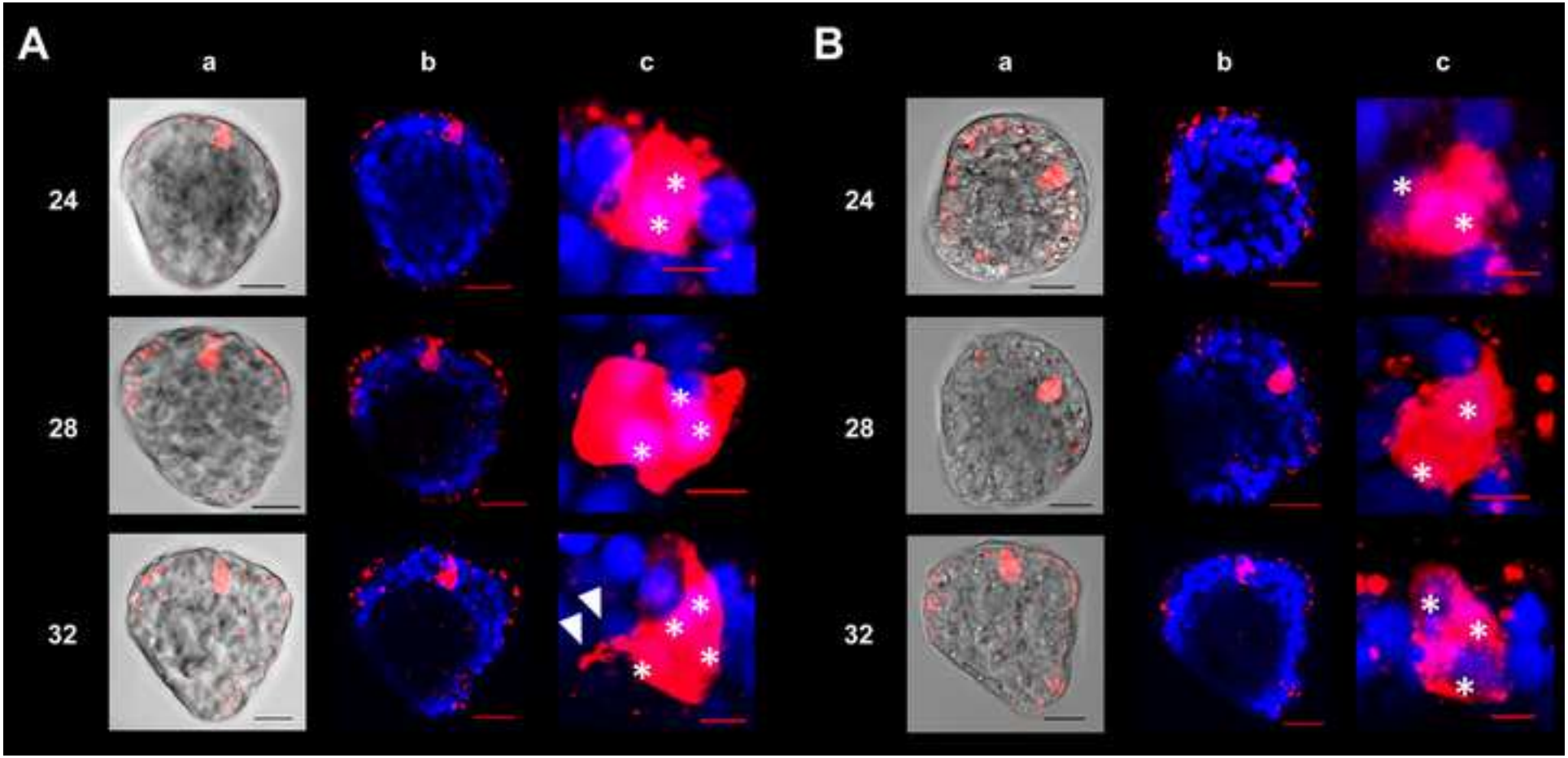

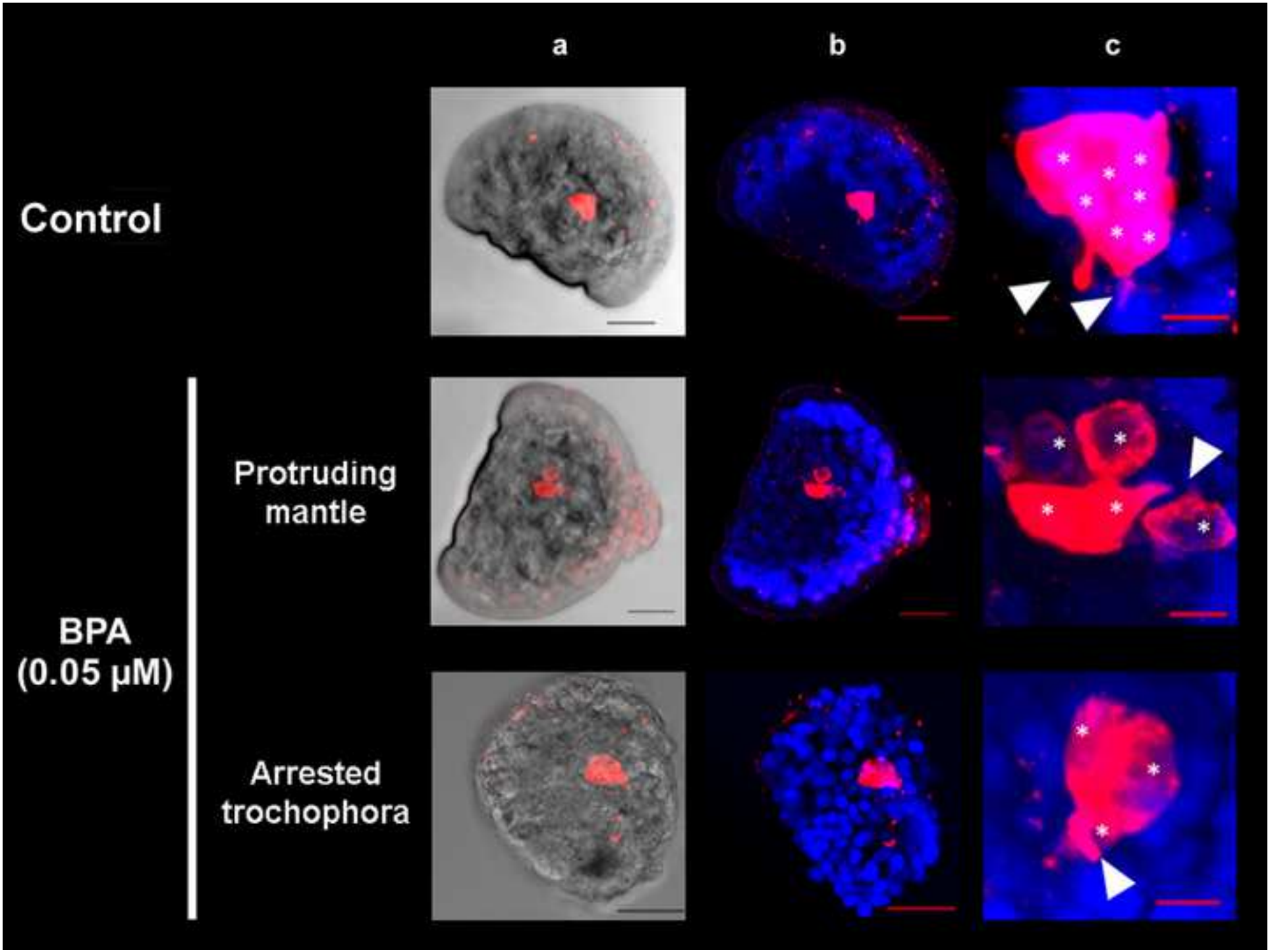

Credit Author Statement

LC, AM, RD, TB conceived the experiments. AM, TB, LB, performed experiments. AM, RD, TB, LC writing and editing. LC supervision. All authors have read and agreed to the published version of the manuscript.

Supplementary material to Miglioli et al.,

Bisphenol A interferes with first shell formation and development of the serotoninergic system in early larval stages of *Mytilus galloprovincialis*

Early development of mussel larvae

In bivalve early development, the onset of shell formation, occurs at the end of the gastrulation, when a group of epithelial cells thickens, forming the shell field. These cells transiently invaginate, forming the shell gland during early trochophore stage (generally from 20 hpf), a swimming larva characterized by two rows of cilia. The trochophora larval body is divided by the prototroch, the equatorial band of ciliated cells, into a pre-trochal area, characterized by the apical tuft, and a post-trochal area distinguished by the presence on the dorsal of the shell forming tissue, the shell field, on the dorsal side of the larva. The shell gland subsequently evaginates and the shell field spreads by flattening of the cells and by mitotic divisions, thus becoming the calcifying mantle. The peripheral cells of the shell gland, that are not internalized during invagination, produce an extracellular lamella – the future periostracum, whose function is to provide the organic matrix support for initial mineral deposition. The evagination is accompanied by the extension in size of the periostracum. Between the periostracum and the cells of the shell field, the primary mineralization takes place. From 28 hpf, shell growth proceeds until 32 hpf: he early shell, the prodissoconch I, exhibits a granular aspect and develops during the late trochophore stage. By this time, the shell field has completed its evagination defining the hinge axis and the body organization undergoes a dramatic change, the larva assuming a triangular shape characteristic of the early veliger stage, characterized by the velum (ciliated swimming and feeding organ). It is followed by the prodissoconch II stage, formed during the D-veliger stage at 48 hpf. The prodissoconch II shell is characterized by concentric growth lines, which mark a change in the calcifying regime.

References

Marin F. 2012 The formation and mineralization of mollusk shell. Frontiers in Bioscience S4, 1099–1125. (doi:10.2741/s321)

Methods

Animal handling, gamete collection and fertilization

Sexually mature specimens of *M. galloprovincialis* were collected from a natural population in the Bay of Villefranche-sur-mer (43.682°N, 7.319°E - France) during the spawning season of 2018/19 (December-March). Animals were kept and maintained at the Institut de la Mer de Villefranche

(IMEV) by the Centre de Ressources Biologiques Marines of the institute (CRBM), transferred to the laboratory and acclimatized in flow-through vessels containing filtered natural seawater MFSW (Millipore filtered seawater) (pH 7.9-8.0, 38 ppt salinity, 15°C). Gametes were obtained by spontaneous spawning; egg quality (shape, size) and sperm motility were checked using an inverted microscope. Sperm and eggs were kept at 16°C until fertilization, that was carried out with an egg:sperm ratio of 1:10. After 30 min, fertilization success (n. fertilized eggs/n. total eggs x 100) was verified by microscopic observation (usually > 90%) and fertilized eggs were transferred to culture vessels at a density of 200 larvae mL^{-1}.

Calcofluor/Calcein staining

Stock solutions of Calcein (4 M in Dimethyl-sulfoxide/DMSO) were diluted in MFSW at 4 mM (4x final concentration). Calcofluor (UV channel, Exc: 408 nm/Em: 450–490 nm) was added to each single well at the time of sampling and prior to fixation (final concentration 0.02 mM in 0.01% DMSO), as previously described (Miglioli et al., 2019). In each well, aliquots of 0.5 mL of 4x Calcein (FITC channel, Exc: 488 nm/Em: 520–560 nm) solution and 1 mL of 2x the BPA solution were added to 0.5 mL of fertilized egg suspension (0.01% DMSO in MFSW) to reach the final nominal concentrations (0.05 0.5, 5 µM BPA and 1 mM calcein – 0.01% DMSO) in a 2 mL volume. Concentrations of BPA in test solutions were checked by solid-phase extraction SPE/LC/MS as previously described (Fabbri et al., 2014, Balbi et al., 2016).

Larval growth at 48 hpf

At 48 hpf, the effect of BPA was also evaluated by scoring shell malformations and measuring shell lengths in larvae from 5 independent parental pairs and in at least 50 larvae for each parental pair. The frequency of shell malformations (% values) and mean shell lengths (µm) were measured. A larva was considered normal when the shell was D-shaped (straight hinge) and the mantle did not protrude out of the shell, and malformed if the larva had not reached the stage typical for 48 h (trocophore or earlier stages) or when some developmental defects were observed (concave,

malformed or damaged shell, protruding mantle) (Fabbri et al., 2014). The acceptability of test results was based on control samples for a percentage of normal D-shell stage larvae >75% (ASTM, 2012).

qPCR

The larval suspension was centrifuged at 800x g for 10 min at 4°C and the obtained pellets were lysed in 1 mL of TRI Reagent (Sigma Aldrich, Milan, Italy). Total RNA was extracted following the manufacturer's instructions (SigmaAldrich, Milan, Italy). RNA concentration and quality were verified using the Qubit RNA assay (Thermo Fisher, Milan, Italy) and electrophoresis using a 1.5% agarose gel under denaturing conditions. First strand cDNA for each sample was synthesized from 1 µg total RNA (Balbi et al., 2016). Primers pairs employed for qPCR analysis and their accession numbers in GenBank were: tyrosinase-TYR [KC878467.1], forward CGATTCTTTATACATGAAATCTGTG-reverse AAACCGTTATAACAACGTGCTAA; serotonin receptor-5-HTR [AB526218], forward CAGCTGCAAGATCGAGGATT-reverse TGAAGCCATCTTGACTGACG. qPCR reactions were performed in triplicate in a final volume of 15 µL containing 7.5 µL iTaq universal master mix with ROX (BioRad Laboratories, Milan, Italy), 5 µL diluted cDNA and 0.3 µM specific primers. A control lacking cDNA template (no-template) was included in the qPCR analysis to determine the specificity of target cDNA amplification. Amplifications were performed in a StepOne real time PCR system apparatus using a standard 'fast mode' thermal protocol (Thermo Fisher, Milan, Italy). Melting curves were utilized for each target mRNA in order to verify the specificity of the amplified products and the absence of artefacts. Dilution series of cDNA were used to calculate the amplification efficiency of each primer pair. HEL and EF-α1 were used for data normalization as the best performing combination of reference gene products (EF1/HEL) (Balbi et al., 2016). Analyses were performed on at least four independent mRNA samples. Calculations of relative expression of target mRNAs was performed by a comparative CT method (Schmittgen and Livak, 2008) using the StepOne software tool (Thermo Fisher). Data are reported as fold changes observed within each life stage with respect to unfertilized eggs in control and BPA-exposed samples.

Figures

Figure S1 - Counting of immunoreactive cells stained with anti-serotonin antibody (5-HT-*ir* cells) in a 48 hpf D-veliger from control conditions. The figure shows a montage of sequential z-stacks of 5-HT-*ir* staining (in red) and Hoechst (in blue) merged on the image. Numbers indicate the nuclei and white arrowheads indicate the emerging neurites. Z-distance between 2 images is 0.9 µm. Scale bars: 5 µm. The nucleus of cell 1 is visible from z1 to z6, cell 2 from z3 to z12, cell 3 from z6 to z13, cell 4 from z12 to z15, cell 5 from z13 to z19, cell 6 from z15 to z16, cell 7 from z20 to z24. Emerging neurites are visible in z1-z2 and in z19.

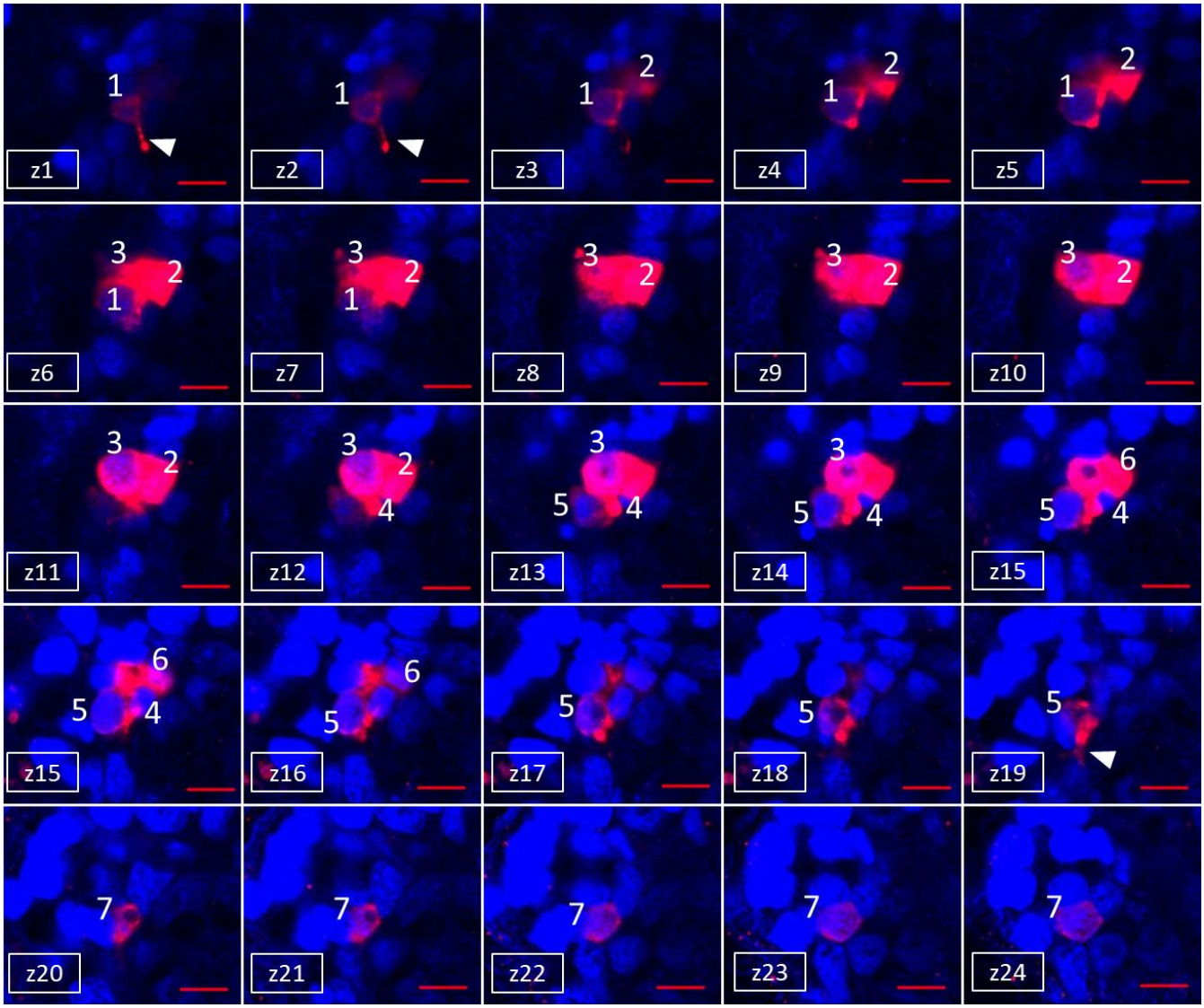

Figure S2 - Immunolocalization of 5-HT-*ir* cells in a mussel larva at 24 hpf (trocophora, lateral view). 5-HT-*ir* cells are shown as red fluorescence, the perimeter of the shell field is indicated in blue. The trochophora larval body is divided into a pre-trochal (on top) and post-trochal region by the prototroch, the equatorial band of ciliated cells. The pre-trochal area is characterized by the

apical tuft (black arrowhead), while the post-trochal area by the presence of the shell forming tissue, the shell field, on the dorsal side of the larva (in blue). 5-HT-*ir* cells (in red) are located in the pre-trochal area, close to the apical tuft. The perimeter of the growing shell and 5-HT-*ir* cells are placed on the opposite sides of the larva: as the shell always grows on the dorsal side, 5-HT-*ir* cells are located ventrally. Scale bar : 20 µm.

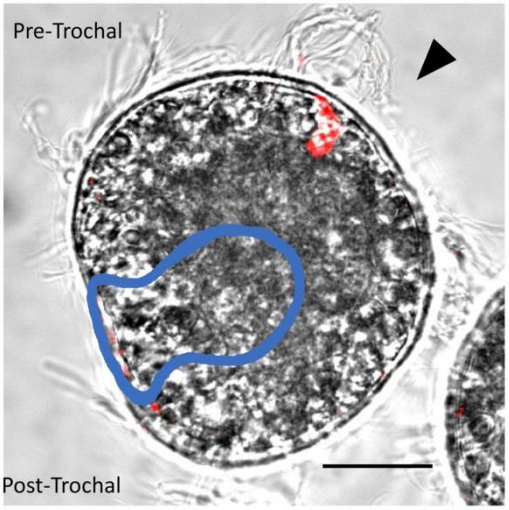

Figure S3 - Effect of BPA (0.5 µM) on serotonin immunoreactivity (5-HT-*ir*) in early larval stages of *M. galloprovincialis* from 24 to 32 hpf. For control images, refer to Fig. 8. All details as in Fig. 8. In BPA-exposed larvae only one 5-HT-*ir* cells could be observed at 24hpf and two cells at 28 and 32 hpf. Scale bars: 20 µm.

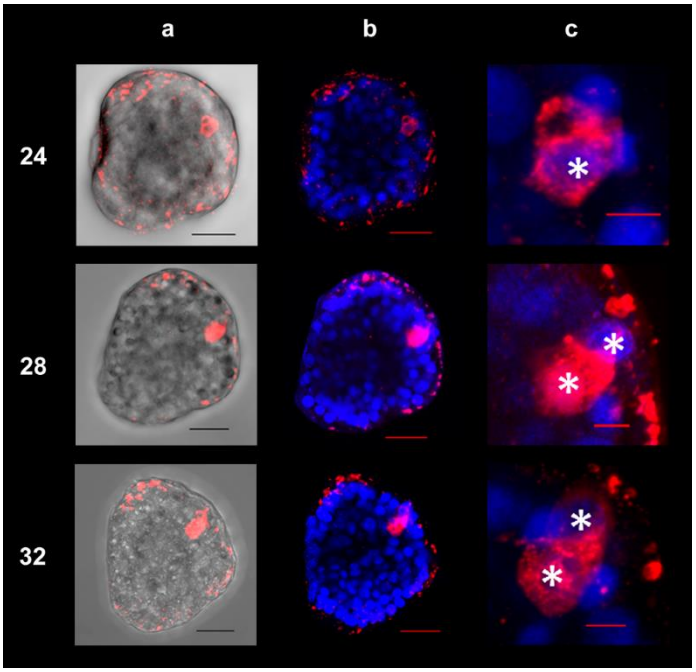

Figure S4 - Effect of BPA (0.5 µM) on serotonin immunoreactivity (5-HT-*ir*) in early larval stages of *M. galloprovincialis* at 48 hpf. All details as in Fig. 9. In BPA-exposed larvae phenotypic alterations were associated with a reduction in the number of 5-HT-*ir* neurons (three in indented hinge, four in protruding mantle and two in arrested trocophora, respectively). Scale bars: 20 µm.